Quantum Dot Superlattice Thermoelectric Materials and Devices

T. C. Harman, P. J. Taylor, M. P. Walsh, B. E. LaForge

PbSeTe-based quantum dot superlattice structures grown by molecular beam epitaxy have been investigated for applications in thermoelectrics. We demonstrate improved cooling values relative to the conventional bulk $(Bi,Sb)_2(Se,Te)_3$ thermoelectric materials using a n-type film in a one-leg thermoelectric device test setup, which cooled the cold junction 43.7 K below the room temperature hot junction temperature of 299.7 K. The typical device consists of a substrate-free, bulk-like (typically 0.1 millimeter in thickness, 10 millimeters in width, and 5 millimeters in length) slab of nanostructured PbSeTe/PbTe as the n-type leg and a metal wire as the p-type leg.

Solid-state thermoelectric (TE) cooling and electrical power generation devices have many attractive features compared with other methods of refrigeration or electrical power generation, such as long life, no moving parts, no emissions of toxic gases, low maintenance, and high reliability. However, their use has been limited by the relatively low energy conversion efficiency of present thermoelectrics. Quantum dot superlattice (QDSL) structures, which have a delta-function distribution of density of states and discrete energy levels due to three-dimensional quantum confinement, a potentially more favorable carrier scattering mechanism, and a much lower lattice thermal conductivity, provide the potential for better thermoelectric devices. The molecular beam epitaxial (MBE) growth of self-assembled QDSL materials on planar substrates using the Stranski-Krastanov growth mode yields improved TE figures of merit (*1*, *2*). Self-assembled quantum dot materials represent just one of a number of new approaches (*3*) being investigated in order to enhance TE performance. Here, we describe the fabrication of a cooling device in a test setup from nanostructured film materials and the device's characteristics obtained from such material. We also discuss the growth and properties of n-type and p-type QDSL film TE materials and background information on the band structure and properties of PbSnSeTe alloy materials (in which the 300 K energy gap can approach zero) [see supporting online material (SOM) Text]. Also presented in the SOM Text are results that indicate conservatively estimated intrinsic ZT values of 2.0 at 300 K have been obtained for PbSnSeTe. Further improvements are anticipated, because both the QDSL materials and devices are not optimized.

Characterization of thermoelectrics. Both the efficiency and coefficient of performance of a TE device are directly related to the dimensionless materials (or intrinsic) figure of merit ZT.

$$ZT = S^2T/\rho\kappa \quad (1)$$

where T is the temperature, S is the Seebeck coefficient or thermopower, ρ is the electrical resistivity, and κ is the thermal conductivity (which includes both the electronic and lattice contributions) used to characterize thermoelectrics. Conventional TE cooling materials are bulk solid solution alloys of Bi_2Te_3, Bi_2Se_3, and Sb_2Te_3, with the best materials having ZT room temperature values of approximately 1.0 (*4*). In order to enhance ZT, a high Seebeck coefficient, an increased electrical conductivity, and a decreased thermal conductivity are needed, but these materials properties often counter each other. Previously, epitaxially grown PbSeTe/PbTe (ternary) QDSL yielded estimated 300 K TE figure of merits of 0.9 (*1*, *2*). The results here indicate that our initial objective of demonstrating that high ZT values (measured in the 1.3 to 1.6 range at 300 K) are possible with QDSL materials and that PbSeTe-based QDSL materials are capable of achieving larger temperature differential values than conventional bulk $(Bi,Sb)_2(Se,Te)_3$ solid solution alloys. It is helpful to define an extrinsic or operating device thermoelectric figure of merit as

$$Z_dT = S_u^2T/R_uK_u \quad (2)$$

Z_dT is reduced from the intrinsic ZT by extraneous or parasitic factors such as those listed below. S_u is the sum of the absolute values of the n-type and p-type Seebeck coefficients; R_u is the total electrical resistance and includes both the thermoelement resistances and the contact resistances; and $K_u$is the total thermal conductance including the thermoelement thermal conductances, junction, or contact thermal conductance, as well as other parasitic effects, such as thermal radiation absorbed on the surfaces around the cold junction surface areas and heat absorption at the cold junction from the thermocouple lead wires used to measure the cold junction temperature. If the parasitics are negligible, then Z_dT for a standard unicouple can be optimized by adjustments in device geometry, which makes R_uK_u a minimum. This requirement leads to $(R_n/K_n) = (R_p/K_p)$, where $R_u = R_n + R_p$ and $K_u = K_n + K_p$ (R_n and R_p are the electrical resistances of the individual n-type and p-type thermoelements, respectively; K_n and K_p are the thermal conductances of the individual n-type and p-type thermoelements, respectively). The intrinsic ZT for a unicouple with negligible parasitics can be written as

$$ZT=(S_p-S_n)^2T/[\sqrt{(\rho_p\kappa_p)}+\sqrt{(\rho_n\kappa_n)}]^2 \quad (3)$$

Bi_2Te_3-alloys are not competitive with large-scale commercial cooling and power generation applications based on fluids and gases. TE ZT values greater than 3.0 are needed to have the potential to compete even in a small part of this market. Nevertheless, niche applications for bulk TE devices have developed, such as small portable refrigerators and picnic coolers and the cooling and temperature stabilization of diode lasers.

Performance characteristics of a TE cooler device. The net rate of transfer of heat or cooling rate (*5*), E_c, out of the cold junction region of a unicouple device structure with electrical current flowing is defined as

$$E_c = S_uT_cI–I^2R_u/2–K_u\Delta T \quad (4)$$

ΔT is the difference in temperature between the hot junction temperature, T_h, and the cold junction temperature, T_c; i.e, $T_h - T_c$. I is the electrical current flowing through each TE element of the device. The thermoelements are connected electrically in series and thermally in parallel. If Eq. 4 is solved for ΔT, it is seen that the ΔT is increased upon adjusting experimental conditions such that $E_c \sim 0$ and I is increased until ΔT reaches a maximum. The maximum attainable temperature difference, ΔT_{max}, may be determined by maximizing Eq. 4 with respect to I_u. This leads to the condition

$$I_u^* = S_uT_c/R_u \quad (5)$$

By inserting Eq. 5 in Eq. 4 and using $E_c = 0$, we obtain the well-known result

$$\Delta T_{max} = (S_uT_c)^2/2R_uK_u \quad (6)$$

Upon using Eqs. 2 and 6, we obtain

$$\Delta T_{max} = Z_dT_c^2/2 \quad (7)$$

Quadratic Eq. 7 can be solved for T_c to yield the minimum attainable temperature $T_{c\,min} = (\sqrt{1+2Z_dT_h}-1)/Z_d$. The above equa-

Lincoln Laboratory, Massachusetts Institute of Technology, Lexington, MA 02420, USA.

tions assume that S_u,R_u, and K_u are averaged quantities over the entire ΔT range.

Fabrication and characteristics of the film TE cooling device. For the device demonstration performed, n-QDSL sample B (Table 1) which was MBE grown on a 18 mm by 18 mm BaF_2 substrate wafer, was used as the starting material. On another wafer from the same n-QDSL growth run B, a Seebeck coefficient of –208 μV/K and an electrical resistivity of 1.71 mΩ-cm were measured (Table 1). n-QDSL B has an unknown thermal conductivity that is determined in the device test setup described here. The n-QDSL B film/BaF_2 substrate wafer was cleaved to size and the 11 mm by 0.104 mm ends immediately metallized in a glove box that contained an inert atmosphere so that oxide formation on the cleaved sample surfaces was minimized. After cleaving, the measured dimensions of the n-QDSL B film were a thickness of 0.104 mm, length of 5.0 mm, and width of 11.0 mm for the n-type TE leg. Then the BaF_2 substrate was removed by dissolution. A gold ribbon 25 μm thick and 250 μm wide with a length of 5 mm was used in place of the conventional p-type TE leg. Gold is a p-type metal (an n-type metal wire would have worked as well) with a 300K Seebeck coefficient of +2.9 μV/K, electrical resistivity of 2.4 μΩ -cm, and a thermal conductivity of 2800 mW/cm-K with a ZT of 0.0.

Table 1. 300 K thermoelectric properties of Bi-doped (n-type) QDSL $PbSe_{0.98}Te_{0.02}$/PbTe samples grown by MBE and an n-type BiSbSeTe alloy sample.

Sample	S(μV/K)	ZT	Carrier conc. (cm^{-3})	Carrier mobility (cm^2/V-s)
n-QDSL A	–219	1.6*	1.2×10^{19}	370
n-QDSL B	–208	1.3*	1.1×10^{19}	300
n-BiSbSeTe A	–228	0.9**	4.6×10^{19}	110

*Values based on thermal conductivity values of 5.8 mW/cm-K calculated from the QDSL device test data. **Value based on a measured thermal conductivity value of 13.6 mW/cm-K.

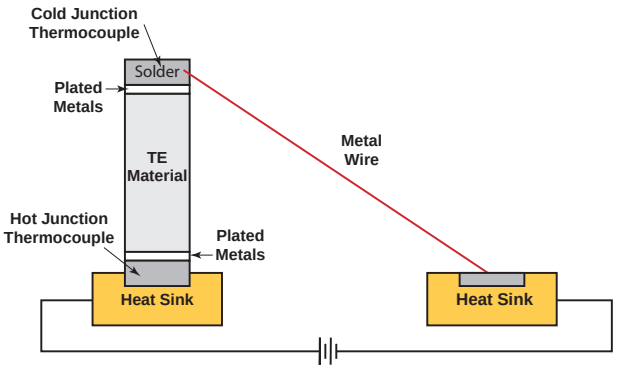

Fig. 1. Schematic of the one-leg thermoelectric cooling device test setup. The setup consists of a thermoelement (TE) with plated metals at both ends of the slab. One end of the TE has a cold junction thermocouple (TC) and a metal wire soldered to the metallized layer. The hot junction end of the TE is soldered to a copper heat sink. A TC is embedded in the solder. The other end of the metal wire is soldered to the second massive copper heat sink. An electrical current source is connected to the two copper heat sinks.

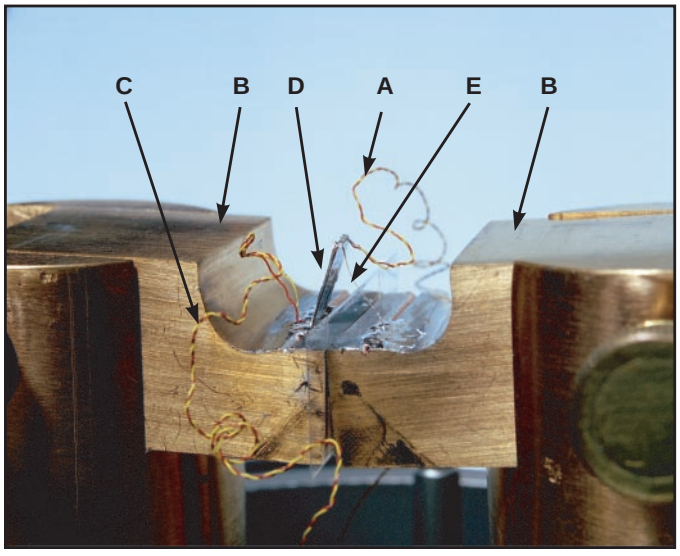

Fig. 2. Photograph of a one-leg thermoelectric refrigerator cooling device test setup made from MBE grown thick film QDSL material. (**A**) Cold junction TC [TC consisted of a twisted pair of chromel (yellow)/alumel (red) wires] soldered to the copper block and metallized end region of the TE. (**B**) Copper heat sinks, which also act as electrical conductors. (**C**) Hot junction thermocouple wires stuck in the soldered end region of the metallized TE. (**D**) MBE grown film QDSL TE. (**E**) Gold ribbon that connects the cold junction region to one of the copper heat sunk blocks. A mylar foil electrically insulates the one copper heat sink block from the other copper heat sink block.

A schematic of the generic one-leg TE refrigerator test setup is shown (Fig. 1). The bulk thermoelectric device made from a thick film of n-type PbSeTe/PbTe QDSL material (current flow in-plane of QD superlattice) is displayed as a photograph (Fig. 2). Not shown is the enclosure of the test device, which enables a good vacuum of about 10^{-5} Torr to be achieved within the chamber containing the device. ΔT versus I data was collected and is shown in graphical form (Fig. 3). The TE demonstration test device cooled the cold junction region to a temperature T_c = 43.7 K below the hot junction temperature, which was maintained at approximately T_h =299.7 K by large copper heat sinks. (Good metal plating and good soldering techniques are necessary in order to obtain high ΔT_{max} values). The T_c thermocouple (TC) is embedded in the liquid solder used to join the T_c TC to the thermoelement and positioned as close to the metallized layer as possible (Fig. 2). The T_h TC was also embedded in liquid solder. Chromel/alumel thermocouples (type K) with a wire diameter of 0.015 cm and a length of 17 cm were used to measure T_h and T_c. Care was taken to ensure that the electrical current had no influence on the TC measurements. Tests were performed on the demonstration device to monitor the TC reading with and without electrical current flowing, and zero voltage pickup by the TC was confirmed. TCs were soldered to both the T_c and the junction with the heat sink to measure T_c and T_h. The electrical current for ΔT_{max} = 43.7 K was 700 mA, and the electrical power input was 87 mW. The ΔT_{max} = 43.7 K temperature differential (without any forced heat removal by blowing air or running water) was much greater than the recently reported value of ΔT_{max} = 32.2 K for a similar single one-leg Bi_2Te_3/Sb_2Te_3 superlattice device (cross-plane current flow of superlattice and no quantum dots) that has an equivalent hot junction temperature (*6*).

To obtain an indication of the parasitic heat flows in our test setup, we used a n-type bulk $(Bi,Sb)_2(Se,Te)_3$ solid solution alloy material (*7*, *8*). The $(Bi,Sb)_2(Se,Te)_3$ alloy sample has a measured 300 K Seebeck coefficient of –228 μV/K, electrical resistivity of 1.24 mΩ-cm, and a thermal conductivity of 13.6 mW/cm-K with a 300 K materials ZT = 0.9 (Eq. 1). A gold ribbon was again used for the p-type leg. Because all materials properties have been measured for this unicouple, the intrinsic

$(ZT)_{one\text{-}leg}$ = 0.34 (Eq. 3) for the $(Bi,Sb)_2(Se,Te)_3$ alloy/Au unicouple. If we made a unicouple of the n-type thermoelement and an identical p-type thermoelement, then $(ZT)_{two\text{-}leg}$ = 0.9 (Eq. 3); i.e., the intrinsic $(ZT)_{two\text{-}leg}$ of the latter device would be a factor of 2.65 larger than the former $(ZT)_{one\text{-}leg}$ device. For the case of no parasitics, the intrinsic ΔT_{max} = 38.8 K (Eq. 6) for the one-legged $(Bi,Sb)_2(Se,Te)_3$ alloy/Au unicouple device (*5*). If we made a unicouple of the n-type thermoelement and an identical p-type thermoelement, then the intrinsic $\Delta T_{two\text{-}leg\ max}$ = 75.6 K (Eq. 6); i.e., the intrinsic $\Delta T_{one\text{-}leg\ max}$ of the latter device would be a factor of two larger than the former $\Delta T_{one\text{-}leg\ max}$ device. The $(Bi,Sb)_2(Se,Te)_3$ alloy material was cleaved to approximately the same aspect ratio L/A as the QDSL material (where A is the cross-sectional area and L is the length of a TE leg) from a bulk, homogeneous single crystal quaternary alloy, which was grown and characterized at the University of Virginia (*8*), the contacts metallized, and the ΔT versus I data was collected. The test device cooled the cold junction region to a temperature (T_c) 30.8 K (lower arrow in Fig. 3) below the hot junction temperature (T_h), which was maintained at 297.7 K by large copper heat sinks. It is believed that the extrinsic $\Delta T_{one\text{-}leg\ max}$ = 30.8 K is 8 K lower than the intrinsic $\Delta T_{one\text{-}leg\ max}$ primarily because of parasitics.

Calculations for n-QDSL A (Table 1) using Eq. 3 indicate that a p-type QDSL leg with TE properties identical to the n-type would yield a QD unicouple with an intrinsic ZT of approximately 1.6, which corresponds to intrinsic $\Delta T_{two\text{-}leg\ max}$ = 103 K with T_h = 300 K. We expect greater cooling differential to be obtained in the future, as compared to our present unoptimized device made from the first bulk-like thick film of PbSeTe/PbTe nanostructured material, by using quaternary QDSL material for n-type and a similarly high ZT p-type leg. The calculated maximum cooling values from 300 K for a standard intrinsic two-leg TE "refrigerator" versus the 300 K intrinsic ZT values are displayed (Fig. 4). The thermal conductivity of the QDSL material was calculated as follows: First, Z_dT = 0.40 was calculated using Eq. 7 from ΔT_{max} = 43.7 K and T_c = 256 K measurements. Then, using extrinsic Z_dT = 0.40 and assuming $Z = Z_d$ in Eq. 3, we calculate the only unknown, i.e., κ of the QDSL material, as κ = 5.8 mW/cm-K. Z cannot be less than Z_d. A higher Z than Z_d would result in an even lower κ. Upon subtracting the electronic part, we obtain 3.3 mW/cm-K for the lattice thermal conductivity of the QDSL sample. For the $(Bi,Sb)_2(Se,Te)_3$ solid solution alloy sample, Eq. 7 yields extrinsic Z_dT = 0.26. Assuming $Z = Z_d$ in Eq. 3, we calculate κ = 20.6 mW/cm-K, which does not agree with the κ value measured on the material at the University of Virginia using a comparison method (with quartz as a reference material) due to parasitics. A second method was used to measure the total thermal conductivity for the two devices. This method (*9*, *10*) uses ΔT versus I data (Fig. 3) at low electrical currents (0 to 25 mA for both polarities of the current). The defining equation is

$$S_u I T_{av} = K_u \Delta T \qquad (8)$$

where T_{av} is the average temperature. The I^2R term can be ignored in Eq. 4 because Joule heating is negligible at such small electrical currents. There are advantages of this method, even when one end of the sample is held in contact with a heat sink (*11*), as in these experiments. The average values (for both polarities of the electrical current) for the I and ΔT data for the n-QDSL B sample are 0, 10.2, 25.2 mA and 0, 1.3, 3.2 K, respectively. The average values (for both polarities of the electrical current) for the I and ΔT data for the Bi_2Te_3-based alloy sample are 0, 10.2, 25.2 mA and 0, 1.0 , 2.45 K, respectively. Applying the data to Eq. 8, we obtain κ = 6.2 mW/cm-K for the n-QDSL B sample. Similarly, κ =15.9 mW/cm-K is derived for the n-type bulk $(Bi,Sb)_2(Se,Te)_3$ solid solution alloy sample. The second method needs high ZT's and good contacts in order to obtain reasonable values for κ. Also, the above κ values are uncorrected for K dependent parasitics (*4*, *10*, *11*). An estimate of the *K*s and *R*s of the two test devices was obtained by calculating the intrinsic or mate-

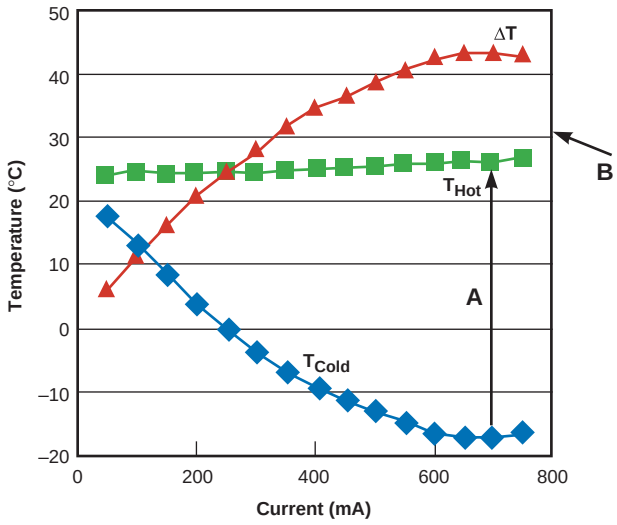

Fig. 3. Thermoelectric cooling characteristics (*T* versus *I*) of one-leg device made from MBE grown thick film QD material and a gold ribbon. The red curve represents measured data points of temperature differential between the hot and cold junction temperatures versus the electrical current flowing through the device. The green curve represents the measured T_h versus I. The blue curve represents the measured T_c versus I. (**A**) Maximum temperature differential of 43.7 K measured for the QDSL TE. (**B**) Maximum temperature differential of 30.8 K measured for the conventional n-type bulk $(Bi,Sb)_2(Se,Te)_3$ solid solution alloy TE material in the same test setup, the same T_h, and approximately the same aspect ratio.

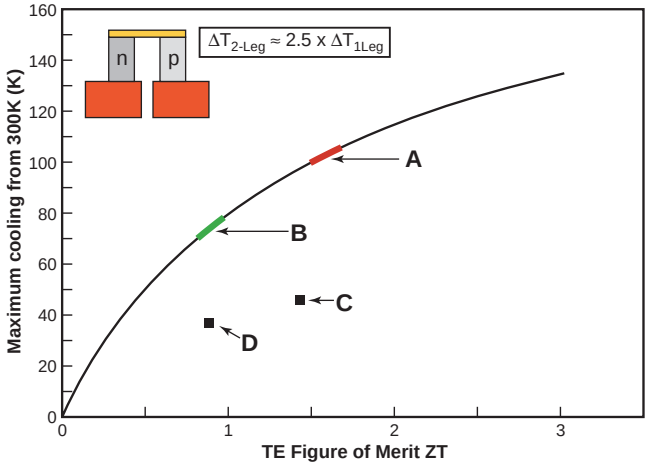

Fig. 4. Thermoelectric maximum temperature differentials versus 300 K ZT for a standard two-leg TE cooler (the standard two good thermoelectric thermoelements fabricated as a unicouple or array of unicouples). Thermoelectric maximum temperature differentials plotted against the 300 K ZT for the two one-legged TE coolers (one good thermoelectric thermoelement used with a second gold wire thermoelement as a unicouple) described in the text. The $\Delta T_{two\text{-}leg} \sim 2.5 \times \Delta T_{one\text{-}leg}$ means that the temperature differential from a two-legged device with equal materials properties is approximately 2.5 times as large as the one-legged device because of the effects of the gold wire on the materials ZT (see Eq. 3). (**A**) Present Pb-salt quantum-dot superlattice materials with identical n- and p-type legs. (**B**) Commercial bulk $(Bi,Sb)_2(Se,Te)_3$ solid solution alloy TE material. (**C**) Present $\Delta T_{one\text{-}leg}$ measured for QDSL/metal wire device with parasitic losses. (**D**) Present $\Delta T_{one\text{-}leg}$ measured for bulk $(Bi,Sb)_2(Se,Te)_3$/metal wire device with parasitic losses.

rials values of $K_{uQDSL/Au} = K_{QDSL} + K_{Au}$, $K_{u(Bi,Sb)_2(Se,Te)_3/Au} = K_{(Bi,Sb)_2(Se,Te)_3} + K_{Au}$, $R_{uQDSL/Au} = R_{QDSL} + R_{Au}$, and $R_{u(Bi,Sb)_2(Se,Te)_3/Au} = R_{u(Bi,Sb)_2(Se,Te)_3} + R_{Au}$, from the measured thermoelectric properties of the individual thermoelements and their dimensions for the two devices as 0.00044 W/K, 0.00061 W/K, 0.094 Ω, and 0.074 Ω, respectively. The calculated K_u's and R_u's are first-order estimates of the actual values, and many factors may change their values, such as the quality of the plating and soldering techniques used to form electrical contacts.

Conclusions. TE cooling test devices have been made from PbSeTe/PbTe QDSL material. 43.7 K of cooling below room temperature was measured, even though one leg was a zero ZT gold wire. This compares to 30.8 K of cooling for the conventional $(Bi,Sb)_2(Se,Te)_3$ material in the same test setup and the same hot junction temperature and about the same aspect ratio. We believe a TE material has been found that is a better room temperature cooler material than bulk $(Bi,Sb)_2(Se,Te)_3$ solid solution alloy material. Device measurements indicate the attainment of device Z_dT and a materials or intrinsic ZT in the range of 1.3 to 1.6 at room temperature. The enhanced TE device performance at 300 K of the PbSeTe/PbTe QDSL material is believed to be (at this point in time) almost entirely due to a high density of quantum nanodots with essentially 100% PbSe composition embedded in a three-dimensional slab matrix of PbTe. As described in the SOM, the first quaternary PbSnSeTe QDSL TE materials have been grown by MBE and have conservatively estimated intrinsic ZT values of 2.0 at 300 K. Further improvements are anticipated, as both the materials and devices are not optimized.

References and Notes

1. T. C. Harman, P. J. Taylor, D. L. Spears, M. P. Walsh, *J. Electron. Mater. Lett.* **29**, L1 (2000).
2. _____, in *18th International Conference on Thermoelectrics*: ICT Symposium Proceedings, Baltimore, MD (IEEE, Piscataway, NJ, 1999), pp. 280–284.
3. M. S. Dresselhaus, in *Recent Trends in Thermoelectric Materials Research III, Semiconductors and Semimetals*, T. W. Tritt, vol. Ed, R. K. Willardson, E. R. Weber, series Eds. (Academic Press, London, 2001), vol. 71, chap. 1. See also the other four chapters in vol. 71, as well as vols. 69 and 70.
4. R. M. Rowe, Ed., *CRC Handbook of Thermoelectrics* (CRC Press, Boca Raton, FL, 1995).
5. T. C. Harman, J. M. Honig, *Thermoelectric and Thermomagnetic Effects and Applications* (McGraw-Hill, New York, 1967), p. 291.
6. R. Venkatasubramanian, E. Sivola, T. Colpitts, B. O'Quinn, *Nature* **413**, 597 (2001).
7. W. M. Yim, F. D. Rosi, *Solid-State Electron.* **15**, 1121 (1972).
8. P. J. Taylor, thesis, Univ. of Virginia (1993).
9. T. C. Harman, *J. Appl. Phys.* **29**, 1373 (1958).
10. _____, J. H. Cahn, M. J. Logan, *J. Appl. Phys.* **30**, 1351 (1959).
11. G. S. Nolas, J. Sharp, H. J. Goldsmid, *Thermoelectrics* (Springer-Verlag, Berlin, 2001), p. 100.
12. W. L. Liu, T. Borca-Tasciuc, G. Chen, J. L. Liu, K. L. Wang, *J. Nanosci. Nanotechnol.* **1**, 39 (2001).

13. Sponsored by the Department of the Navy and the Defense Advanced Research Projects Agency (DARPA) under Air Force contract no. F19628-00-C-0002. The opinions, interpretations, conclusions, and recommendations are those of the authors and are not necessarily endorsed by the Department of Defense.

Supporting Online Material
www.sciencemag.org/cgi/content/full//297/5590/2229/DC1
SOM Text
References and Notes
Fig. S1
Tables S1, S2, S3

15 April 2002; accepted 28 August 2002

Establishment and Maintenance of a Heterochromatin Domain

Ira M. Hall,[1,2]* Gurumurthy D. Shankaranarayana,[1]* Ken-ichi Noma,[1]* Nabieh Ayoub,[3] Amikam Cohen,[3] Shiv I. S. Grewal[1,2]†

The higher-order assembly of chromatin imposes structural organization on the genetic information of eukaryotes and is thought to be largely determined by posttranslational modification of histone tails. Here, we study a 20-kilobase silent domain at the mating-type region of fission yeast as a model for heterochromatin formation. We find that, although histone H3 methylated at lysine 9 (H3 Lys[9]) directly recruits heterochromatin protein Swi6/HP1, the critical determinant for H3 Lys[9] methylation to spread in cis and to be inherited through mitosis and meiosis is Swi6 itself. We demonstrate that a centromere-homologous repeat (*cenH*) present at the silent mating-type region is sufficient for heterochromatin formation at an ectopic site, and that its repressive capacity is mediated by components of the RNA interference (RNAi) machinery. Moreover, *cenH* and the RNAi machinery cooperate to nucleate heterochromatin assembly at the endogenous *mat* locus but are dispensable for its subsequent inheritance. This work defines sequential requirements for the initiation and propagation of regional heterochromatic domains.

In eukaryotes, the organization of chromatin into higher-order structures governs diverse chromosomal processes. Besides creating distinct metastable transcriptional domains during cellular differentiation, the formation of higher-order chromatin domains is widely recognized to be essential for imprinting, dosage compensation, recombination, and chromosome condensation (*1–4*). The assembly of heterochromatin at centromeres is essential for the accurate segregation of chromosomes during cell division, and the formation of such specialized structures at telomeres protects chromosomes from degradation and from aberrant chromosomal fusions (*2*). Moreover, repetitive DNA sequences such as transposable elements are often assembled into heterochromatin that, in addition to its role in transcriptional repression, maintains genome integrity by suppressing recombination between repetitive elements (*5*).

The posttranslational modification of histone tails plays a causal role in the assembly of higher-order chromatin, and accumulating evidence suggests that patterns of histone modification specify discrete downstream regulatory events (*6, 7*). The factors that define particular chromosomal domains as preferred sites of heterochromatin assembly are largely uncharacterized. It has been suggested that heterochromatin protein complexes are preferentially targeted to repetitive DNA elements, such as commonly found at the pericentric heterochromatin and intergenic regions of higher eukaryotes (*8, 9*). Interestingly, rather than any specific sequence motif, the repetitive nature of transgene arrays alone appears to be sufficient for heterochromatin formation (*9, 10*). Furthermore, studies of position effect variegation have shown that heterochromatin complexes possess the ability to spread along the chromosomes, resulting in the heritable inactivation of nearby sequences (*2*).

Higher-order chromatin structure is critical for the functional organization of centromeres and the mating-type region of the fission yeast *Schizosaccharomyces pombe* (*2*). At centromeres, tandem and inverted arrays of the *dg* and *dh* centromeric repeats surrounding the unique central core are assembled into heterochromatin and are bound by CENP-B proteins that resemble the trans-

[1]Cold Spring Harbor Laboratory, [2]Watson School of Biological Sciences, Post Office Box 100, Cold Spring Harbor, NY 11724, USA. [3]Department of Molecular Biology, The Hebrew University-Hadassah Medical School, Jerusalem, Israel 91010.

*These authors contributed equally to this work.
†To whom correspondence should be addressed. E-mail: grewal@cshl.org

Quantum Dot Superlattice Thermoelectric Materials and Devices

T. C. Harman *et al.*

Science **297**, 2229 (2002);
DOI: 10.1126/science.1072886

Science (print ISSN 0036-8075; online ISSN 1095-9203) is published weekly, except the last week in December, by the American Association for the Advancement of Science, 1200 New York Avenue NW, Washington, DC 20005.